

In A. Kuijper, K. Bredies, T. Pock, H. Bischof (Eds.): Scale-Space and Variational Methods in Computer Vision. Lecture Notes in Computer Science, Vol. 7893, pp. 210-221, Springer, Berlin, 2013. The final publication is available at link.springer.com.

Why is the Census Transform Good for Robust Optic Flow Computation?

David Hafner, Oliver Demetz, and Joachim Weickert

Mathematical Image Analysis Group,
Faculty of Mathematics and Computer Science,
Campus E1.7, Saarland University, 66041 Saarbrücken, Germany
{hafner,demetz,weickert}@mia.uni-saarland.de

Abstract. The census transform is becoming increasingly popular in the context of optic flow computation in image sequences. Since it is invariant under monotonically increasing grey value transformations, it forms the basis of an illumination-robust constancy assumption. However, its underlying mathematical concepts have not been studied so far. The goal of our paper is to provide this missing theoretical foundation. We study the continuous limit of the inherently discrete census transform and embed it into a variational setting. Our analysis shows two surprising results: The census-based technique enforces matchings of extrema, and it induces an anisotropy in the data term by acting along level lines. Last but not least, we establish links to the widely-used gradient constancy assumption and present experiments that confirm our findings.

Keywords: robust optic flow, census transform, illumination changes, anisotropy, variational method

1 Introduction

In 1994, Zabih and Woodfill have proposed the so-called *census transform* [1]. It computes for every pixel a binary string (*census signature*) by comparing its grey value with the grey values in its neighbourhood. In particular, the signature encodes whether the neighbours are smaller than the reference pixel or not. For a 3×3 neighbourhood, the census signature has length 8 and can be represented efficiently via a single byte.

The census transform is becoming increasingly important: It provides an illumination-robust constancy assumption for solving correspondence problems in computer vision, e.g. computation of the displacement field (*optic flow*) in image sequences. The census signatures are by construction *morphologically invariant*, i.e. invariant under global monotonically increasing grey level rescalings.

This can be an important advantage in modern applications such as driver assistant systems. Stein [2] uses the census signatures in an efficient feature matching approach. A hash table-based indexing scheme provides flow estimates in real-time and is well-suited for large displacements. Müller et al. [3] as well as Mohamed and Mertsching [4] exploit these sparse feature matches to handle large displacements and to recover image details lost in a coarse-to-fine minimisation technique, respectively. Furthermore, Müller et al. [5] embed the census transform as a data term into a variational optic flow framework. Tests in real-world scenarios show the desired morphological invariance of the resulting dense flow fields. Also in the context of stereo estimation, Ranftl et al. [6] have demonstrated the usefulness of the census-transform under challenging lighting conditions.

In spite of its increasing popularity, however, the theoretical understanding of the successful census transform is still rather limited.

Our Contributions. The goal of our paper is to provide a thorough theoretical foundation of the census transform. Our contributions are threefold:

- (i) We regard differences to neighbours as approximations of directional derivatives and study the continuous limit where all possible angles are taken into account.
- (ii) We develop this concept into a constancy assumption, and we embed it as data term in a variational model for optic flow computation.
- (iii) Most importantly, we analyse the energy functional and its minimisation in order to obtain a novel interpretation of census-based optic flow. We will see that this interpretation reveals many clever properties of the census transform which have not been used in other optic flow formulations.

We want to stress that the focus of our work is not on developing new competitive high-end optic flow methods: We are interested in a mathematical underpinning of census-based approaches. Once their properties are well-understood, these ideas can easily be embedded in any highly sophisticated optic flow method that ranks favourably in the Middlebury benchmark [7].

Related Work. Since 1994, the census idea has appeared under several names in the literature: Ojala et al. [8] developed almost the same concept independently but interpreted the resulting descriptor as a binary number (*local binary patterns*). Later, Calonder et al. [9] revisited this idea by introducing the feature point descriptor *BRIEF*.

There is also a long tradition of designing methods for illumination-robust optic flow computation. Inspired by Uras et al. [10], Brox et al. [11] achieve robustness w.r.t. additive brightness changes by considering the image gradients in addition to the intensity values. Chambolle and Pock [12] follow a different strategy to tackle these additive illumination changes and estimate the additive component explicitly. Another idea by Mileva et al. [13] is to make use of photometric invariants to design illumination-robust flow methods for colour images.

Paper Organisation. Starting with a continuous interpretation of the census transform, Section 2 presents our census-based variational optic flow method. The energy formulation and its minimisation yield new insights into census-based approaches. These results are presented in Section 3. After having sketched our numerical algorithm in Section 4, we evaluate the proposed method in Section 5. Finally, Section 6 concludes the paper with a summary and an outlook.

2 Census-Based Variational Optic Flow

In this section, we introduce our census-based optic flow method. To this end, we start with a formal definition of the original census transform and derive the corresponding constancy assumption in a continuous manner. This provides the basis of our energy functional and is the starting point of our analysis.

2.1 Census Transform

Let in a discrete setting $g_{i,j}$ denote the grey values of an image. Then, every digit of the census signature in pixel $(i, j)^\top$ is computed as

$$H(g_{i+d_1, j+d_2} - g_{i,j}), \quad (1)$$

where $(i + d_1, j + d_2)^\top$ is a neighbouring pixel, and $H: \mathbb{R} \rightarrow \{0, 1\}$ denotes the Heaviside step function

$$H(z) := \begin{cases} 0 & \text{if } z < 0 \\ 1 & \text{if } z \geq 0 \end{cases}. \quad (2)$$

2.2 Census-Based Constancy Assumption

Let us now transfer the census transform to the continuous setting and derive the associated constancy assumption. For this purpose, the three-dimensional function $f(x, y, t)$ represents a spatio-temporal image sequence, where $(x, y)^\top$ describes the location within the rectangular image domain $\Omega \subset \mathbb{R}^2$ and $t \in [0, T]$ denotes the time.

The argument of the step function in Equation (1) approximates a directional derivative. Consequently, one census digit can be interpreted as the discrete version of

$$H(\partial_{\mathbf{e}_\varphi} f(x, y, t)), \quad (3)$$

where the directional derivative operator $\partial_{\mathbf{e}_\varphi}$ only acts on the spatial domain. Here, the unit vector $\mathbf{e}_\varphi := (\cos \varphi, \sin \varphi)^\top$ specifies the direction.

We now derive the constancy assumption that corresponding points $(x, y, t)^\top$ and $(x + u, y + v, t + 1)^\top$ in two consecutive frames have identical census signatures. In our notation, the functions $u, v: \Omega \rightarrow \mathbb{R}$ represent the sought optic

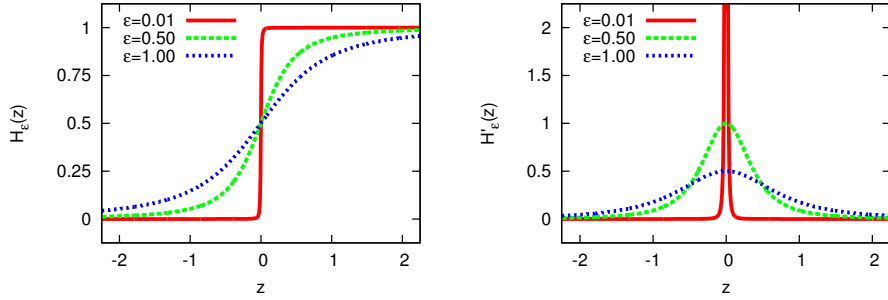


Fig. 1. Different approximations $H_\varepsilon(z)$ of the Heaviside step function (*left*) and corresponding derivatives $H'_\varepsilon(z)$ (*right*). Smaller choices of ε lead to closer approximations of the original sharp step function.

flow. With the abbreviations $\mathbf{x} := (x, y, t)^\top$ and $\mathbf{w} := (u, v, 1)^\top$, the constancy assumption of the census signature implies

$$H(\partial_{e_\varphi} f(\mathbf{x} + \mathbf{w})) - H(\partial_{e_\varphi} f(\mathbf{x})) \stackrel{!}{=} 0 \quad \forall \varphi \in [0, 2\pi). \quad (4)$$

In order to embed this constraint as a data term in an energy functional, we consider a linearised version of it. To this end, we replace the Heaviside step function H by the smooth approximation

$$H_\varepsilon(z) := \frac{1}{2} \left(1 + \frac{z}{\sqrt{z^2 + \varepsilon^2}} \right), \quad (5)$$

with a small positive regularisation parameter $\varepsilon > \varepsilon_0 > 0$ (cf. Figure 1). The numerical parameter ε_0 ensures that ε is also in the limit strictly larger than 0. Otherwise, the linearisation becomes invalid and the resulting data term would not be suitable for a typical variational optic flow framework [14].

Assuming small flow components u and v as well as a small change of the directional derivative $\partial_{e_\varphi} f(\mathbf{x})$ in time, we propose a twofold linearisation of the regularised version of constraint (4). For this purpose, let $\nabla_3 := (\partial_x, \partial_y, \partial_t)^\top$ denote the spatio-temporal gradient and

$$H'_\varepsilon(z) = \frac{\varepsilon^2}{2(z^2 + \varepsilon^2)^{3/2}} \quad (6)$$

the derivative of $H_\varepsilon(z)$. At first, we linearise $\partial_{e_\varphi} f(\mathbf{x} + \mathbf{w})$ around \mathbf{x} and obtain

$$H_\varepsilon(\partial_{e_\varphi} f(\mathbf{x}) + \mathbf{w}^\top \nabla_3(\partial_{e_\varphi} f(\mathbf{x}))) - H_\varepsilon(\partial_{e_\varphi} f(\mathbf{x})) \stackrel{!}{=} 0. \quad (7)$$

In the second step, the first H_ε term in (7) is linearised around $\partial_{e_\varphi} f(\mathbf{x})$:

$$H'_\varepsilon(\partial_{e_\varphi} f(\mathbf{x})) \cdot \mathbf{w}^\top \nabla_3(\partial_{e_\varphi} f(\mathbf{x})) \stackrel{!}{=} 0. \quad (8)$$

2.3 Energy Formulation and Minimisation

Now, we embed the derived constancy assumption into a variational framework. To this end, let $\nabla := \nabla_2 := (\partial_x, \partial_y)^\top$ denote the spatial gradient operator. Furthermore, let $\alpha > 0$ be a regularisation parameter that allows to steer the impact of the data and smoothness term, respectively. Then, an energy incorporating the proposed linearised constancy assumption is given by

$$E(\mathbf{w}) := \int_{\Omega} (M(f, \mathbf{w}) + \alpha \cdot S(\mathbf{w})) \, d\mathbf{x}, \quad (9)$$

with the census-based data term

$$M(f, \mathbf{w}) := \frac{1}{\pi} \int_0^{2\pi} H'_\varepsilon{}^2(\partial_{e_\varphi} f) \cdot (\mathbf{w}^\top \nabla_3(\partial_{e_\varphi} f))^2 \, d\varphi \quad (10)$$

and the quadratic smoothness term

$$S(\mathbf{w}) := |\nabla u|^2 + |\nabla v|^2. \quad (11)$$

For the sake of clarity, we omit the argument \mathbf{x} of the functions f , u , and v . Following the calculus of variations, the minimiser of the energy in Equation (9) w.r.t. u and v has to fulfil the Euler-Lagrange equations

$$\frac{1}{\pi} \int_0^{2\pi} H'_\varepsilon{}^2(\partial_{e_\varphi} f) \cdot \partial_{e_\varphi} f_x \cdot \mathbf{w}^\top \nabla_3(\partial_{e_\varphi} f) \, d\varphi - \alpha \Delta u = 0, \quad (12)$$

$$\frac{1}{\pi} \int_0^{2\pi} H'_\varepsilon{}^2(\partial_{e_\varphi} f) \cdot \partial_{e_\varphi} f_y \cdot \mathbf{w}^\top \nabla_3(\partial_{e_\varphi} f) \, d\varphi - \alpha \Delta v = 0, \quad (13)$$

with reflecting Neumann boundary conditions $\mathbf{n}^\top \nabla u = 0$ and $\mathbf{n}^\top \nabla v = 0$. Here, \mathbf{n} denotes the outer normal vector to the boundary of Ω .

3 Interpretation

To analyse the presented census-based data term in Equation (10), we exploit the symmetry of the integrand w.r.t. π and the equivalence $\partial_{e_\varphi} f = e_\varphi^\top \nabla f$ for differentiable functions f :

$$M(f, \mathbf{w}) = \frac{2}{\pi} \int_0^\pi H'_\varepsilon{}^2(e_\varphi^\top \nabla f) \cdot (\mathbf{w}^\top \nabla_3(e_\varphi^\top \nabla f))^2 \, d\varphi. \quad (14)$$

Further algebraic rearrangements allow to isolate the *census tensor* \mathbf{C} :

$$M(f, \mathbf{w}) = \frac{2}{\pi} \int_0^\pi H'_\varepsilon{}^2(e_\varphi^\top \nabla f) \cdot \left(e_\varphi^\top \begin{pmatrix} \mathbf{w}^\top \nabla_3 f_x \\ \mathbf{w}^\top \nabla_3 f_y \end{pmatrix} \right)^2 \, d\varphi \quad (15)$$

$$= \begin{pmatrix} \mathbf{w}^\top \nabla_3 f_x \\ \mathbf{w}^\top \nabla_3 f_y \end{pmatrix}^\top \cdot \underbrace{\frac{2}{\pi} \int_0^\pi H'_\varepsilon{}^2(e_\varphi^\top \nabla f) e_\varphi e_\varphi^\top \, d\varphi}_{=: \mathbf{C}} \cdot \begin{pmatrix} \mathbf{w}^\top \nabla_3 f_x \\ \mathbf{w}^\top \nabla_3 f_y \end{pmatrix}. \quad (16)$$

A thorough analysis of this symmetric tensor $\mathbf{C} \in \mathbb{R}^{2 \times 2}$ has already been performed by Weickert in the context of anisotropic diffusion filtering [15]. Here, we review the results that are relevant for us: Let $(r, \psi)^\top$ denote the polar coordinates of $\nabla f \neq \mathbf{0}$. Then, Weickert has shown that the first and second eigenvector of \mathbf{C} are parallel and perpendicular to isolines of f , respectively. They read

$$\mathbf{v}_\parallel(\psi) = \begin{pmatrix} -\sin \psi \\ \cos \psi \end{pmatrix} \quad \text{and} \quad \mathbf{v}_\perp(\psi) = \begin{pmatrix} \cos \psi \\ \sin \psi \end{pmatrix}, \quad (17)$$

and the corresponding eigenvalues are

$$\lambda_\parallel(r) = \frac{4}{\pi} \int_0^{\frac{\pi}{2}} H'_\varepsilon{}^2(r \cos \varphi) \cdot \sin^2 \varphi \, d\varphi, \quad (18)$$

$$\lambda_\perp(r) = \frac{4}{\pi} \int_0^{\frac{\pi}{2}} H'_\varepsilon{}^2(r \cos \varphi) \cdot \cos^2 \varphi \, d\varphi. \quad (19)$$

Let us now substitute the census tensor \mathbf{C} in (16) by its eigendecomposition

$$\mathbf{C} = \lambda_\parallel(r) \cdot \mathbf{v}_\parallel(\psi) \mathbf{v}_\parallel^\top(\psi) + \lambda_\perp(r) \cdot \mathbf{v}_\perp(\psi) \mathbf{v}_\perp^\top(\psi). \quad (20)$$

Thus, we obtain

$$M(f, \mathbf{w}) = \lambda_\parallel(r) \cdot \left(\mathbf{v}_\parallel^\top(\psi) \begin{pmatrix} \mathbf{w}^\top \nabla_3 f_x \\ \mathbf{w}^\top \nabla_3 f_y \end{pmatrix} \right)^2 + \lambda_\perp(r) \cdot \left(\mathbf{v}_\perp^\top(\psi) \begin{pmatrix} \mathbf{w}^\top \nabla_3 f_x \\ \mathbf{w}^\top \nabla_3 f_y \end{pmatrix} \right)^2, \quad (21)$$

where the original data term is explicitly split into two perpendicular constraints. In particular, this can be understood as a projection of the linearised gradient constancy assumption along and across isolines of f . Moreover, both terms are weighted with the corresponding eigenvalues $\lambda_\parallel(r)$ and $\lambda_\perp(r)$.

3.1 Anisotropic Data Term

Based on the formulation in Equation (21), the following two paragraphs discuss the behaviour of the data term at different image regions:

Vanishing Gradient. At extrema and homogeneous regions, where $|\nabla f|$ vanishes ($r \rightarrow 0$), the eigenvalues of the census tensor \mathbf{C} fulfil

$$\lim_{r \rightarrow 0} \lambda_\parallel(r) = \lim_{r \rightarrow 0} \frac{4}{\pi} \int_0^{\frac{\pi}{2}} H'_\varepsilon{}^2(r \cos \varphi) \cdot \sin^2 \varphi \, d\varphi = H'_\varepsilon{}^2(0) \cdot \underbrace{\frac{4}{\pi} \int_0^{\frac{\pi}{2}} \sin^2 \varphi \, d\varphi}_{=1} \quad (22)$$

and accordingly

$$\lim_{r \rightarrow 0} \lambda_\perp(r) = \lim_{r \rightarrow 0} \frac{4}{\pi} \int_0^{\frac{\pi}{2}} H'_\varepsilon{}^2(r \cos \varphi) \cdot \cos^2 \varphi \, d\varphi = H'_\varepsilon{}^2(0) \cdot \underbrace{\frac{4}{\pi} \int_0^{\frac{\pi}{2}} \cos^2 \varphi \, d\varphi}_{=1}. \quad (23)$$

Revisiting Equation (6), we see that $H'_\varepsilon{}^2(0) = \frac{1}{4\varepsilon^2}$. Hence, both eigenvalues λ_\parallel and λ_\perp exceed all bounds for close approximations of the Heaviside function. This means that the gradient constancy is assumed parallel as well as perpendicular to isolines of the image (cf. Equation (21)).

The occurring second order image derivatives $\partial_{e_\varphi} f_x$ and $\partial_{e_\varphi} f_y$ in the Euler-Lagrange Equations (12) and (13) behave differently in local extrema and homogeneous image regions. Consequently, our analysis of the constancy assumption has to differentiate these two cases:

Local Extrema. Here, the first order derivatives vanish, but the second order derivatives are in general non-zero. Since the reaction parts are weighted with the factor $\frac{1}{4\varepsilon^2}$, they dominate the diffusion terms entirely for small ε .

This reveals a surprising property of the discussed census-based model: The constancy assumption implicitly enforces a strong reliance on the local extrema, which contributes to the observed morphological invariance. On the one hand the positions of the minima and maxima remain constant under monotonically increasing grey level rescalings, and on the other hand the property $\nabla f = \mathbf{0}$ at the extrema is not violated under those illumination changes. Thus, the imposed constancy assumption of the gradient holds here in all directions.

Homogeneous Regions. In contrast, the second order image derivatives ∇f_x and ∇f_y go to $\mathbf{0}$ in homogeneous regions. As a result, the terms

$$\partial_{e_\varphi} f_x = e_\varphi^\top \nabla f_x \quad (24)$$

as well as

$$\partial_{e_\varphi} f_y = e_\varphi^\top \nabla f_y \quad (25)$$

in the reaction parts of the Euler-Lagrange equations vanish. Hence, the solution at those regions is solely determined by filling-in the information from the neighbouring pixels:

$$\Delta u = 0, \quad (26)$$

$$\Delta v = 0. \quad (27)$$

High Contrast Edges. The previous paragraph was concerned with image regions where $r \rightarrow 0$. Let us now shed light on the opposite case ($r \rightarrow \infty$), which corresponds to high contrast edges of the image. Considering the eigenvalues of the census tensor \mathcal{C} shows the strong anisotropic behaviour in those regions:

$$\lim_{r \rightarrow \infty} \frac{\lambda_\parallel(r)}{\lambda_\perp(r)} = \infty. \quad (28)$$

This ratio of the eigenvalues has already been analysed by Weickert for a family of monotonically decreasing functions including $H'_\varepsilon{}^2(z)$ [15].

Considering Equation (21), we see that the constancy of the gradient entries is here strongly imposed along isolines of f . In contrast, the constancy assumption

across isolines is weighted down. This anisotropy is, besides the reliance on the local extrema, another reason for the morphological invariance of census-based methods. Under monotonically increasing grey level rescalings, the positions of the isophotes are invariant and additionally the directional derivatives along these isophotes remain zero. In other words, the gradient constancy assumption is valid in this direction.

3.2 Relation to the Gradient Constancy Assumption

Let us now illustrate the connection between the presented census-based constancy assumption and the widely-used gradient constancy assumption [10, 11]. The data term of the linearised gradient constancy assumption reads

$$(\mathbf{w}^\top \nabla f_x)^2 + (\mathbf{w}^\top \nabla f_y)^2 = \begin{pmatrix} \mathbf{w}^\top \nabla_3 f_x \\ \mathbf{w}^\top \nabla_3 f_y \end{pmatrix}^\top \mathbf{I} \begin{pmatrix} \mathbf{w}^\top \nabla_3 f_x \\ \mathbf{w}^\top \nabla_3 f_y \end{pmatrix}, \quad (29)$$

where \mathbf{I} denotes the 2×2 identity matrix. This formulation inherently decouples the constancy assumptions of the gradient entries f_x and f_y . Comparing the data terms (16) and (29), we observe that the reason for the increased robustness of census-based methods (compared to gradient constancy) is hidden in the census tensor \mathbf{C} . This confirms our findings from Section 3.1: Coupling the constancy assumptions of f_x and f_y by \mathbf{C} , or rather by its eigenvectors $\mathbf{v}_\parallel(\psi)$ and $\mathbf{v}_\perp(\psi)$, induces an anisotropic behaviour which effects the proposed invariance.

Replacing the regularised step function H_ε in Equation (16) by the identity function, the matrix \mathbf{C} comes down to

$$\frac{2}{\pi} \int_0^\pi 1 \cdot \mathbf{e}_\varphi \mathbf{e}_\varphi^\top d\varphi = \frac{2}{\pi} \int_0^\pi \begin{pmatrix} \cos^2 \varphi & \cos \varphi \sin \varphi \\ \sin \varphi \cos \varphi & \sin^2 \varphi \end{pmatrix} d\varphi = \frac{2}{\pi} \begin{pmatrix} \frac{\pi}{2} & 0 \\ 0 & \frac{\pi}{2} \end{pmatrix} = \mathbf{I}. \quad (30)$$

The resulting data term coincides with the gradient constancy assumption in Equation (29). Consequently, the census-based method may be regarded as a *censorisation* of the gradient constancy. On the one hand, this censorisation decreases the amount of extracted image information due to the binary quantisation of the directional derivative values. On the other hand, however, the induced anisotropy increases the robustness under illumination changes. While the original gradient constancy assumption is solely invariant w.r.t. global additive illumination changes, the *censored* gradient constancy assumption provides an invariance against any kind of monotonically increasing grey level rescalings.

4 Implementation

For the ease of implementation, we cast the linearised constancy assumption from (8) into the versatile motion tensor framework by Bruhn [16]. To this end, we exploit the equivalence

$$H'_\varepsilon(\partial_{\mathbf{e}_\varphi} f) \cdot \mathbf{w}^\top \nabla_3(\partial_{\mathbf{e}_\varphi} f) = \mathbf{w}^\top \nabla_3 H_\varepsilon(\partial_{\mathbf{e}_\varphi} f). \quad (31)$$

Furthermore, we approximate the periodic integral in Equation (10) by the Riemann sum and finally obtain

$$M(f, \mathbf{w}) = \mathbf{w}^\top \left(\frac{2}{N} \sum_{n=0}^{N-1} \nabla_3 H_\varepsilon(\partial_{\mathbf{e}_{\varphi_n}} f) \cdot \nabla_3^\top H_\varepsilon(\partial_{\mathbf{e}_{\varphi_n}} f) \right) \mathbf{w}, \quad (32)$$

where N denotes the number of considered neighbours and $\varphi_n := 2\pi \frac{n}{N}$. Choosing e.g. $N = 8$, the direct neighbours of each pixel are used to compute the census signatures. Generally, we assume the images to be sampled on a regular grid with horizontal and vertical grid sizes h_1 and h_2 , respectively. Accordingly, the directional derivative $\partial_{\mathbf{e}_{\varphi_n}} f$ at pixel $(i, j)^\top$ is approximated via the two point stencil

$$[\partial_{\mathbf{e}_{\varphi_n}} f]_{i,j} = \frac{[f]_{i+d_1, j+d_2} - [f]_{i,j}}{\sqrt{(h_1 d_1)^2 + (h_2 d_2)^2}}, \quad (33)$$

where the vector $\mathbf{d} := (d_1, d_2)^\top \neq \mathbf{0}$ represents, especially for diagonal neighbours, a scaled version of \mathbf{e}_{φ_n} (cf. Section 2.1). All other spatial and temporal derivatives are computed by means of standard finite differences.

The resulting discrete versions of the Euler-Lagrange Equations (12) and (13) create a sparse linear system of equations, which we solve iteratively using a variant of the Gauß-Seidel method, namely successive over-relaxation [17].

5 Evaluation

Our experiments have been performed on the commonly available test image sequence *New Marble*¹. We subjected the grey values $g \in [0, 255]$ of the second input image to the monotonically increasing transformation

$$g_{\text{out}} = 255 \cdot \left(\frac{m \cdot g_{\text{in}} + a}{255} \right)^\gamma, \quad (34)$$

where the constant a represents additive changes, $m > 0$ multiplicative changes and $\gamma > 0$ is used for gamma corrections.

The parameter ε of the regularised step function should be adapted to the noise level and is here fixed to 0.1. Furthermore, the input images are pre-smoothed with a Gaussian of standard deviation 0.8 and the census signatures are determined on a 3×3 neighbourhood ($N = 8$).

Figure 2 demonstrates the increased robustness of the census-based method compared to the gradient constancy assumption. In the absence of artificial illumination changes (*first column*), the gradient constancy provides a better *average angular error* (AAE) [18]. It extracts more information from the input images. The resulting flow fields for additive changes (*second column*) are unaltered due to the inherent invariance of both methods. In contrast, the gradient constancy assumption is not invariant under multiplicative rescalings and gamma

¹ available from http://i21www.ira.uka.de/image_sequences

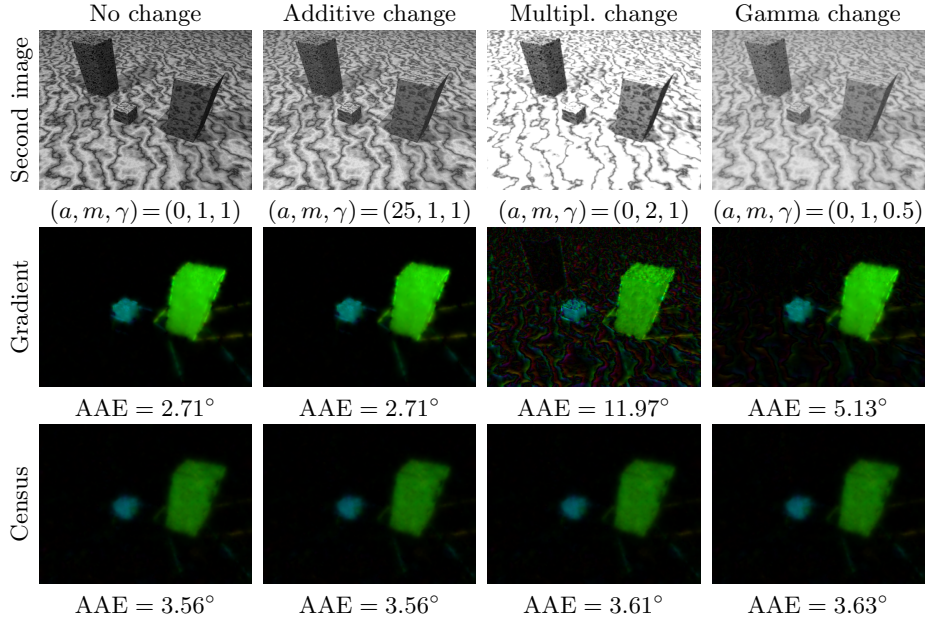


Fig. 2. Visual comparison of the gradient constancy assumption (*second row*, $\alpha=430$) and its censored version (*third row*, $\alpha=7$) under illumination changes. The second input image (*first row*) is manipulated by different grey level rescalings (cf. Equation (34)).

corrections (*third and fourth column*), while the censored version provides an increased robustness. The absolute invariance is lost due to the presmoothing and ε being unequal to zero.

In addition, the plots in Figure 3 confirm these observations. The gradient constancy is not able to compensate for the multiplicative changes and gamma corrections. Contrary, the census-based approach provides the proposed robustness. However, this increase of robustness is associated with a loss of accuracy in the presence of small illumination changes.

6 Conclusions and Future Work

We have seen that interpreting the census transform in the continuous limit and embedding it into a variational framework reveals unexpected insights. The presented census-based technique shows two key properties: the strong reliance on local extrema as well as the restriction of the gradient constancy assumption along level lines. These advanced features are efficiently realised by a very simple binary transform. They exploit the morphological invariance of the gradient direction in a clever way and yield the observed robustness under illumination changes. This builds the basis for the success of the census transform in the context of correspondence problems.

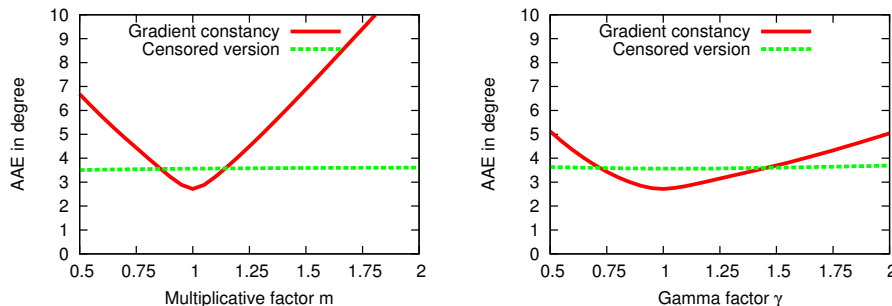


Fig. 3. Comparison of the gradient constancy assumption and its censored version under global multiplicative illumination changes (*left*) and gamma corrections (*right*). The parameter setting can be found in Figure 2.

These promising insights motivate us to investigate also generalisations of the census transform that involve higher order constancy assumptions, e.g. constancy of the Hessian. The key properties of the census transform are of course not restricted to optic flow models. They have already proven to be equally beneficial for other computer vision tasks such as stereo reconstruction [6] or face detection [19].

Our findings confirm the general usefulness of studying continuous limits of inherently discrete morphological transforms. Other examples include e.g. continuous reinterpretations of median filters in terms of mean curvature motion [20] and morphological amoebae as self-snakes [21].

Acknowledgements. Our research has partly been funded by the Deutsche Forschungsgemeinschaft (DFG) through the Saarbrücken Graduate School of Computer Science and a Gottfried Wilhelm Leibniz Prize.

References

1. Zabih, R., Woodfill, J.: Non-parametric local transforms for computing visual correspondence. In Eklundh, J.O., ed.: Computer Vision – ECCV ’94. Volume 801 of LNCS. Springer, Berlin (1994) 151–158
2. Stein, F.: Efficient computation of optical flow using the census transform. In Rasmussen, C.E., Bülthoff, H.H., Giese, M.A., Schölkopf, B., eds.: Pattern Recognition. Volume 3175 of LNCS. Springer, Berlin (2004) 79–86
3. Müller, T., Rannacher, J., Rabe, C., Franke, U.: Feature- and depth-supported modified total variation optical flow for 3D motion field estimation in real scenes. In: Proc. 24th IEEE Conference on Computer Vision and Pattern Recognition, Colorado Springs, IEEE Computer Society Press (2011) 1193–1200
4. Mohamed, M.A., Mertsching, B.: TV-L1 optical flow estimation with image details recovering based on modified census transform. In Bebis, G., Boyle, R., Parvin, B., Koracin, D., Charless, F., Wang, S., Choi, M.H., Mantler, S., Schulze, J., Acevedo,

- D., Mueller, K., Papka, M., eds.: *Advances in Visual Computing*. Volume 7431 of LNCS. Springer, Berlin (2012) 482–491
5. Müller, T., Rabe, C., Rannacher, J., Franke, U., Mester, R.: Illumination-robust dense optical flow using census signatures. In Mester, R., Felsberg, M., eds.: *Pattern Recognition*. Volume 6835 of LNCS. Springer (2011) 236–245
 6. Ranftl, R., Gehrig, S., Pock, T., Bischof, H.: Pushing the limits of stereo using variational stereo estimation. In: *IEEE Intelligent Vehicles Symposium*, Alcalá de Henares, IEEE Computer Society Press (2012) 401–407
 7. Baker, S., Scharstein, D., Lewis, J.P., Roth, S., Black, M.J., Szeliski, R.: A database and evaluation methodology for optical flow. *International Journal of Computer Vision* **92**(1) (2011) 1–31
 8. Ojala, T., Pietikäinen, M., Harwood, D.: A comparative study of texture measures with classification based on featured distributions. *Pattern Recognition* **29**(1) (1996) 51–59
 9. Calonder, M., Lepetit, V., Strecha, C., Fua, P.: BRIEF: Binary robust independent elementary features. In Daniilidis, K., Maragos, P., Paragios, N., eds.: *Computer Vision – ECCV 2010*. Volume 6314 of LNCS. Springer, Berlin (2010) 778–792
 10. Uras, S., Girosi, F., Verri, A., Torre, V.: A computational approach to motion perception. *Biological Cybernetics* **60** (1988) 79–87
 11. Brox, T., Bruhn, A., Papenberger, N., Weickert, J.: High accuracy optical flow estimation based on a theory for warping. In Pajdla, T., Matas, J., eds.: *Computer Vision – ECCV 2004*. Volume 3024 of LNCS. Springer, Berlin (2004) 25–36
 12. Chambolle, A., Pock, T.: A first-order primal-dual algorithm for convex problems with applications to imaging. *Journal of Mathematical Imaging and Vision* **40**(1) (2011) 120–145
 13. Mileva, Y., Bruhn, A., Weickert, J.: Illumination-robust variational optical flow with photometric invariants. In Hamprecht, F.A., Schnörr, C., Jähne, B., eds.: *Pattern Recognition*. Volume 4713 of LNCS. Springer, Berlin (2007) 152–162
 14. Horn, B.K.P., Schunck, B.G.: Determining optical flow. *Artificial Intelligence* **17** (1981) 185–203
 15. Weickert, J.: Anisotropic diffusion filters for image processing based quality control. In Fasano, A., Primicerio, M., eds.: *Proc. Seventh European Conference on Mathematics in Industry*. Teubner, Stuttgart (1994) 355–362
 16. Bruhn, A.: *Variational Optic Flow Computation: Accurate Modelling and Efficient Numerics*. PhD thesis, Dept. of Computer Science, Saarland University, Saarbrücken, Germany (2006)
 17. Young, D.M.: *Iterative Solution of Large Linear Systems*. Academic Press, New York (1971)
 18. Barron, J.L., Fleet, D.J., Beauchemin, S.S.: Performance of optical flow techniques. *International Journal of Computer Vision* **12**(1) (1994) 43–77
 19. Fröba, B., Ernst, A.: Face detection with the modified census transform. In: *Proc. 6th IEEE International Conference on Automatic Face and Gesture Recognition*, IEEE Computer Society Press (2004) 91–96
 20. Guichard, F., Morel, J.M.: Partial differential equations and image iterative filtering. In Duff, I.S., Watson, G.A., eds.: *The State of the Art in Numerical Analysis*. Number 63 in IMA Conference Series (New Series). Clarendon Press, Oxford (1997) 525–562
 21. Welk, M., Breuß, M., Vogel, O.: Morphological amoebas are self-snakes. *Journal of Mathematical Imaging and Vision* **39**(2) (2011) 87–99